Triple-Doppler Analysis of a Discretely Propagating, Long-Lived, High Plains Squall Line

RODNEY L. GRADY* AND JOHANNES VERLINDE

Department of Meteorology, The Pennsylvania State University, University Park, Pennsylvania

(Manuscript received 20 June 1996, in final form 28 April 1997)

ABSTRACT

A nonsevere squall line that developed on 21 June 1993 along the northern foothills of the Colorado Rocky Mountains is analyzed using a series of triple-Doppler analyses. This squall line developed in a relatively dry environment characterized by weak low-level but strong upper-level vertical shear of the horizontal winds. The drier thermodynamic profile, as characterized by a higher lifting condensation level, and weak low-level shear resulted in convection forming not along, but rather 7–10 km behind the leading edge of the shallow cold pool. The strong upper-level shear established a predominantly leading anvil. This led to a suppression zone immediately ahead of the leading line, which in turn resulted in a discrete mode of propagation of the squall line. Three different cycles were observed: each cycle had a distinct line of convective cells that initiate, intensify, and then decay. In each case the new cells developed 20–40 km out ahead of the decaying line of the previous cycle.

Many studies have identified low-level shear as being critical to squall line development. Results from this study indicate that there may be a more extensive set of environmental conditions that will lead to long-lived midlatitude squall lines. In particular, the strong upper-level shear played an important role in the characteristics of this storm.

1. Introduction

Much of the precipitation that occurs over the central United States during the summer months occurs at night, and has its roots in thunderstorm activity along the eastern slopes of the Rocky Mountains (Wallace 1975; Maddox 1980). Often this convective activity develops into squall lines, that, in turn, develop into mesoscale convective complexes (MCCs) (Menard and Fritsch 1989; Schmidt and Cotton 1989). Although MCCs contribute most to the total precipitation (Fritsch et al. 1986), Midwestern squall lines constitute a much higher frequency of occurrence. In Oklahoma alone during the span of 11 years for the months of April, May, and June, Bluestein and Jain (1985) and Bluestein et al. (1987) observed the formation of approximately 150 squall lines.

Because of their number and spatial extent, squall lines have traversed many special higher density observational networks, allowing them to be well documented. Most observational studies of midlatitude squall lines document the mature stage when a well-defined stratiform region exists and the squall line has propagated out of its source region (Ogura and Liou 1980; Smull and Houze 1985; Smull and Houze 1987a). However, few case studies have examined the initial stages of squall line development (Bluestein and Jain 1985; Bluestein et al. 1987; Klimowski 1994). In this paper, we investigate the initial stages of a squall line that developed at 1930 UTC 21 June 1993 over the foothills of the Colorado Rocky Mountains in an environment where the vertical wind shear was weak at low- to midlevels but strong at upper levels. The mesoscale convective system (MCS) produced hail 14 mm in diameter and surface wind gusts to 19 m s^{-1} within the first 2½ hours of its existence. This nonsevere squall line was part of a much larger MCS that developed around 1730 UTC 21 June 1993 and persisted until 0800 UTC 23 June, at which time the system had propagated into Minnesota.

Squall lines are typically long-lived meteorological phenomena. Two mechanisms that cause this longevity have been documented. The first mechanism involves persistent propagating updraft and downdraft couplets coexisting within the same line, and was proposed by Browning and Ludlam (1962) and numerically simulated in 2D by Moncrieff and Miller (1976), Thorpe et al. (1982, hereafter TMM), and Miller and Moncrieff (1983). Browning and Ludlam's 2D model was based on a 3D supercell in a deeply sheared environment. In

* Current affiliation: Air Weather Service, Scott Air Force Base, Illinois.

Corresponding author address: Hans Verlinde, Dept. of Meteorology, The Pennsylvania State University, 503 Walker Building, University Park, PA 16802-5013.
E-mail: verlinde at essc.psu.edu

the numerical simulations of TMM, they used a moderate low-level shear environment and found that the developing storm involved only one cell, and so was classified as a ''2D supercell.'' While rotating 3D supercells are frequently observed, 2D supercells have not been documented.

The second mechanism, where the squall line propagates through the redevelopment of ordinary cells, was first observed and postulated by Newton (1950). Since Newton's first observations, many other recent observations validated this mechanism for longevity as commonplace (e.g., Zipser 1977; Leary and Houze 1979; Gamache and Houze 1982; Houze and Hobbs 1982; among others). Smull and Houze (1987a) and Houze et al. (1989) presented a conceptual model of these squall lines. In this model, flow from a slightly upshear-tilted updraft branches into a gradually ascending front-to-rear flow in a predominantly trailing anvil, while another weaker branch flows into the leading anvil. Below the trailing anvil is an area of descending rear-inflow that, coupled with downdrafts, helps to keep a nearly continual source of surface convergence and upward motion along the leading edge of the gust front. Several numerical simulations have successfully reproduced the regeneration propagation mechanism [Dudhia and Moncrieff 1987; Rotunno et al. 1988, hereafter RKW; Fovell and Ogura 1988]. While observations are typically spatially and temporally limited, numerical models afford researchers detail and understanding that is not often possible in a natural environment. From their numerical simulations RKW were able to establish a conceptual model for cell redevelopment and propagation that rested upon the balance between baroclinically generated horizontal vorticity at the cold pool boundary and horizontal vorticity inherent in the ambient vertical low-level wind shear. Along the leading edge of the gust front, the balanced state produced the deepest lifting and was most likely to regenerate strong convective cells. A typical unbalanced state existed when the vorticity induced by an ever-increasing cold pool was greater than the vorticity present in the low-level ambient shear. Simulation in a weakly sheared environment (Weisman et al. 1988; hereafter WKR) resulted in convective cells decaying after 1.5 h, and creating an apparent upshear-tilted updraft by 2 h. Generally speaking, balanced circulations led to longevity and unbalanced circulations led to decay. Many of the observed features within midlatitude squall lines have been explained as a function of this cold pool/low-level ambient shear conceptual model. These features include the tilted updraft and trailing anvil (RKW and WKR), and rear-inflow jet (Weisman 1992). All these studies used a 3D nonhydrostatic model and were initialized with similar idealized ambient environmental conditions. The idealized conditions were horizontally homogeneous and characterized by a single sounding representative of typical squall line environments.

In light of the many inhomogeneities present within the real environment, many differences from the conceptual model and from the numerical simulations are found in observations. Such differences are expected since environmental factors that vary both spatially and temporally create asymmetries within the squall line. Asymmetries in an inhomogeneous environment are normal and are found at any stage of the squall line's life. Houze et al. (1990) documented asymmetries in their study of the radar reflectivity patterns of mature squall lines. Bluestein and Jain (1985) and Bluestein et al. (1987) documented the formative stage of squall lines and found that development into a linearly oriented structure occurred in a variety of ways. Most of these asymmetries still occur within the same general conceptual model advanced by Smull and Houze (1987a) and simulated by RKW, WKR, and Weisman.

The degree to which asymmetries and inhomogeneities are observed is dependent upon a number of factors, including synoptic and mesoscale forcing, atmospheric stability, vertical wind shear, and topography. Under the right set of environmental conditions, the possibility exists to develop an asymmetric, quasi ''2D supercellular'' squall line. The 21 June 1993 squall line is such a case.

The purpose of this investigation is to document a nontypical, asymmetric squall line, compare it with the typical conceptual model in the literature, and to describe several environmental factors that may have contributed to its atypical, asymmetric structure.

2. Data sources and methods of analysis

The data for the analyses were collected from late morning to early afternoon of 21 June 1993 during the NCAR RAPS-93 (Realtime Analysis and Prediction of Storms, 1993) field project. Figure 1 shows the locations of the surface mesonet, wind profilers, radio acoustic sounding system (RASS), rawinsondes, and Doppler radars used in this analysis.

Surface data were collected every 5 min from the NOAA Program for Regional Observing and Forecasting Services (PROFS) mesonet and additional National Center for Atmospheric Research (NCAR) Portable Automated Mesonet (PAM) observing platforms. Surface pressure data were adjusted to 1500 m MSL, and individual station biases were corrected through comparison with National Weather Service (NWS) Standard Airways Observations (SAO). Objective analyses of kinematic fields were accomplished using the mesonet data interpolated to an 8-km grid using a nearest-neighbor analysis grid (Cahir et al. 1981). The 915-MHz Denver/Stapleton wind profiler and companion NOAA/Wave Propagation Laboratory RASS (Strauch et al. 1984) measured the vertical wind structure and the derived virtual temperature profile, respectively. The RASS observations were taken at 150-m intervals through the lowest 1.5 km AGL. To calculate virtual potential temperatures, height coordinates were converted to pressure coordinates by integrating the hydro-

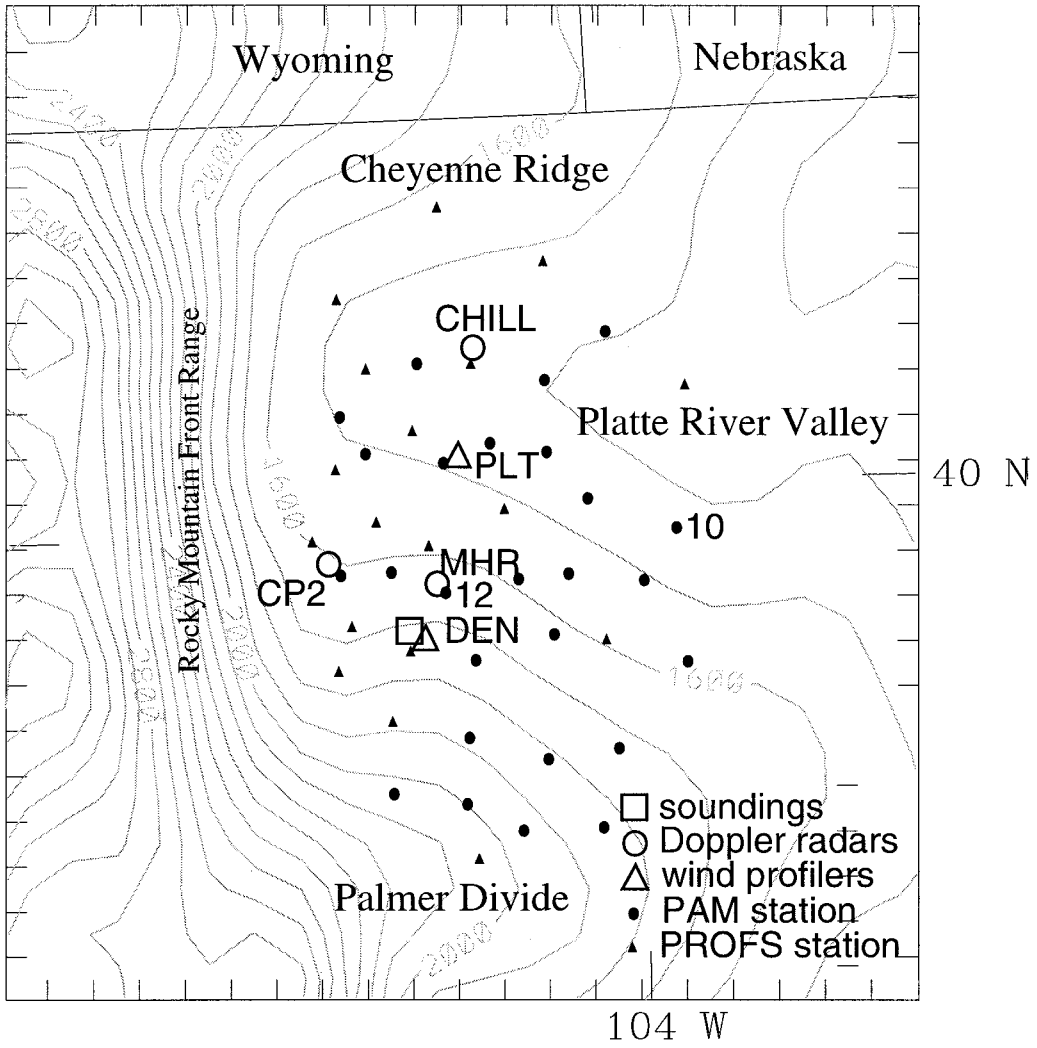

FIG. 1. Topographic map of the RAPS-93 area with instrument locations. The NOAA RASS is collocated with the Denver profiler. The CLASS sounding and the standard NWS Denver sounding were released within 2 km of each other. The terrain contour interval is 100 m.

static equation upward (Neiman et al. 1991), using the surface observation as the lower boundary condition and RASS virtual temperatures as the mean-level temperatures. Standard NWS rawinsonde observations and a supplemental Cross-chain Loran Atmospheric Sounding System (CLASS) sounding were used in calculating vertical environmental quantities.

The S-band radars used in the analysis included the NCAR CP2 and CSU-CHILL Doppler radars, as well as the Mile High Doppler radar (MHR). The dual-Doppler lobes were defined to be the intersection between the area of a between-beam angle, $30° < \theta < 150°$, and the area that provided 1.5-km spatial resolution (Davies-Jones 1979). Reflectivities and Doppler velocities were edited in radar coordinates before being interpolated onto a Cartesian grid. The grid extended up to 14.0 km AGL, with horizontal and vertical spacing of 1.5 and 0.5 km, respectively.

The radial velocity and reflectivity fields were advected to a volume-scan average time. A final composite reflectivity field was developed using the maximum value at each grid point from any of the three radars. The horizontal wind field was calculated from the three radial wind fields using a three-equation solution. Where data from only two of the radars were available, a two-equation solution was implemented. The contribution of the terminal fall velocity to the radial velocity was neglected in the analysis to determine the two horizontal wind components, since elevation angles were generally quite low. A two-step Leise filter was used to smooth the horizontal winds, completely damping all disturbances shorter than four times the horizontal grid spacing, or 6 km. Vertical motions were obtained using a downward integration of the anelastic continuity equation, accounting for particle fall speeds and applying a top boundary condition of zero vertical motion. The

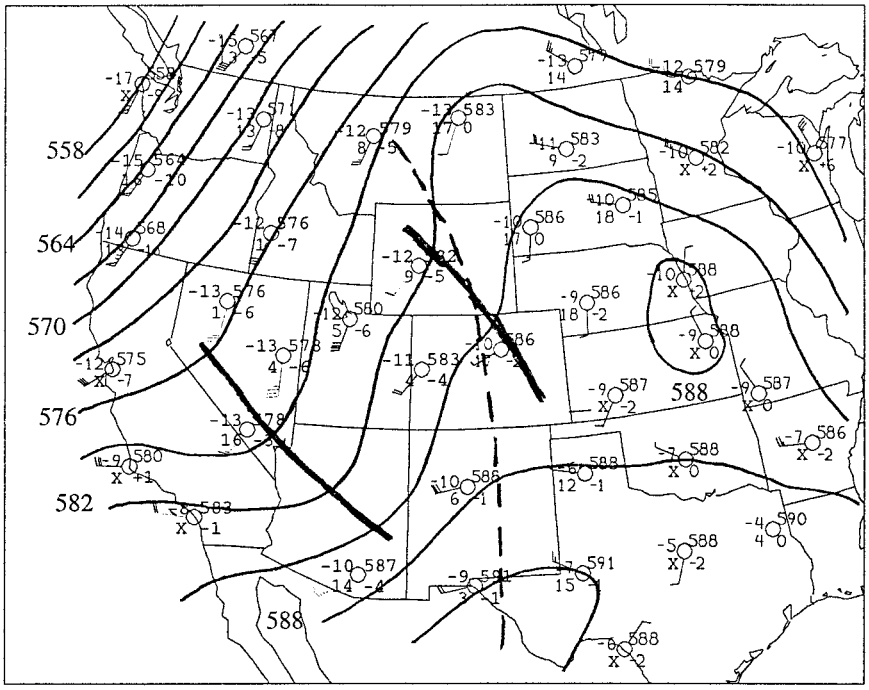

FIG. 2. Upper-air analysis for 1200 UTC 21 June 1993 at 500 hPa. Plotted station parameters include temperature (°C), dewpoint depression (°C), geopotential height (decameters), and 12-h height changes. Geopotential heights (solid) are contoured every 30 m. The trough position is indicated by the thick solid line and the 1200 UTC 21 June 1993 700 hPa thermal ridge is indicated by the thick dashed line.

vertical velocities for the northern end of the convective line are suspect for analyses through 2102 UTC and for portions of analyses 2102–2130 UTC. This is due to CSU-CHILL's maximum elevation scan of 13 deg not resolving storm top while the MCS was in close proximity to the radar. An unresolved storm top does not pose problems to the derived horizontal winds and its derivatives, since at the low elevation scans, the radial velocities measured by the radar were comprised predominantly from the horizontal component of the winds. Squall line motion was determined from the average movement of discernible reflectivity cores. The reflectivity cores and the axis of highest reflectivities within the convective line were observed to move at the same speed and direction (241° at 7.9 m s^{-1}). This movement was subtracted from Doppler-derived winds to yield line relative flow. The average direction varied by 15° and the average speed varied by 1.5 m s^{-1}.

3. System overview

a. Synoptic environment

The 500-hPa analysis for 1200 UTC 21 June (Fig. 2) reveals a short-wave trough (thick solid line) located over Colorado and Wyoming. Satellite images and vorticity analyses helped to identify the trough position upstream from the Colorado Front Range. A time series (not shown) of the horizontal wind profiles at the Platteville wind profiler, located 49 km north of the Denver rawinsonde site, indicated passage of the trough at roughly 1600–1700 UTC. Also present at 1200 UTC was a north to south oriented 700-hPa thermal ridge, shown as the dashed line.

At 1200 UTC a weak south-southwesterly surface flow into a stationary frontal boundary extending across southern Nebraska (not shown) helped keep higher surface dewpoint temperatures over the plains states. The mesonet analysis at this time revealed a broad trough just east of the foothills of the Rockies, with dewpoints ranging from 8° to 11°C and winds light and variable.

A weak Denver cyclone (Szoke et al. 1984) developed, advecting moister air into the mesonet area from the plains of eastern Colorado (Fig. 3), with a further increase in the boundary layer moisture coming from the diurnal increase in latent heat flux. The 12°C dewpoint isopleths at 1200, 1400, and 1700 UTC show an initial increase in area with the isopleth advancing westward from 1200 to 1400 UTC. The isopleth had retreated from its 1400 UTC maximum extension by 1700 UTC, leaving the Front Range area dewpoints 4°–6°C higher than the early morning values.

Two soundings, released at 1200 (Denver NWS) and 1700 UTC (NCAR CLASS sonde), revealed change to the vertical structure of the environment (Fig. 4). The layer between 700 and 450 hPa destabilized with the advancing 700-hPa thermal ridge. A surface-based layer

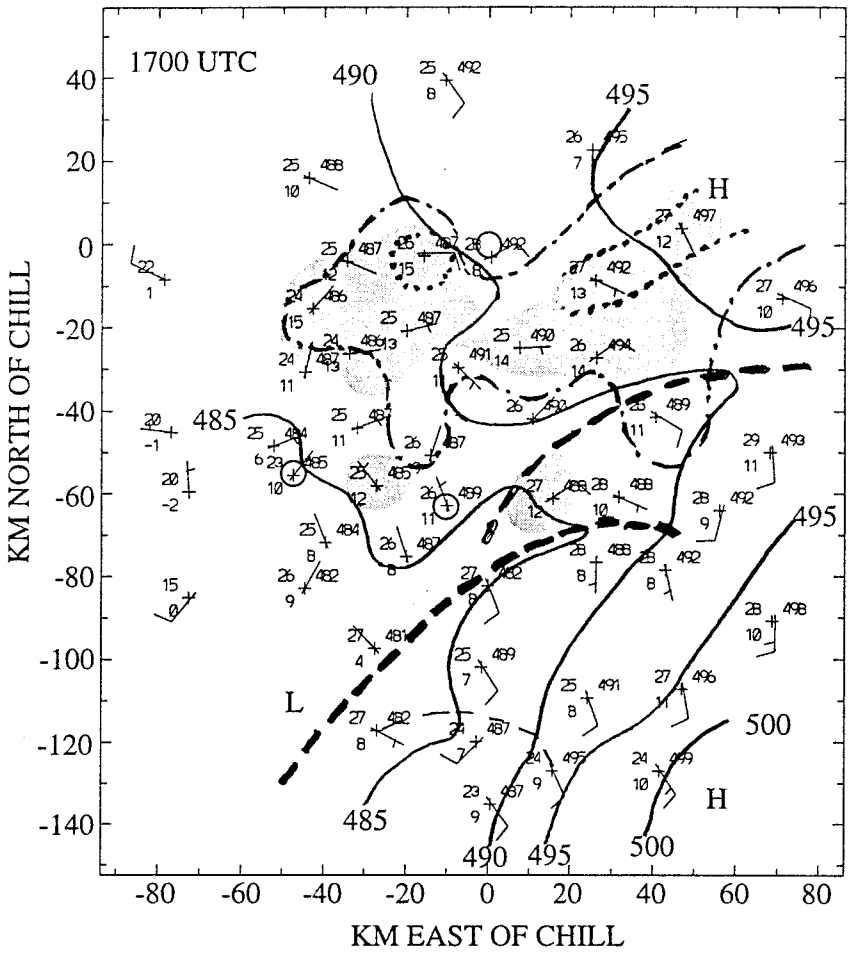

FIG. 3. Surface mesonet analysis for 1700 UTC 21 June 1993. Plotted station parameters include temperature (°C), dewpoint (°C), corrected station pressure adjusted to 1500 m (hPa) multiplied by 10 (with leading 8 dropped), and the wind barbs (full barb = 5 m s^{-1}). Station pressure is contoured at 0.5-hPa intervals. Areas where dewpoints are greater than 12°C are lightly shaded. Also shown are the 12°C isodrosotherms for 1200 (dotted) and 1400 UTC (dash–dotted). The circles identify the location of the three Doppler radars.

of weak east-southeast flow deepened to the 700-hPa level, advecting higher θ_e air into the genesis region. The vertical wind shear was generally weak to 400 hPa in both soundings but increased above this level.

The atmospheric stability was calculated using the surface conditions [temperature 29°C, dewpoint 9°C; also, see Crook (1996)] just prior to convection initiation (1930 UTC) east of the foothills. It was assumed that the middle and upper layers of the atmosphere remained unchanged from the 1700 UTC sounding. The vertical structure of the atmosphere revealed little indication of being able to support long-lived convection: the convective available potential energy was only 1150 J kg^{-1}, vertical wind shear was weak, and the lifting condensation level (LCL) and level of free convection (LFC) were 2.4 km and 3.1 km AGL, respectively. The bulk Richardson number (Weisman and Klemp 1982) was 127, indicative of an environment supportive of multicellular storms.

Initial convection over the Front Range developed at 1730 UTC in association with the slow moving, upper-level short-wave trough. This convection was a subset of a larger system of MCSs oriented northwest to southeast along the Rocky Mountains (Fig. 5a). This larger system propagated eastward as a predominantly linear structure through Nebraska and the Dakotas before decaying in the early morning hours of 23 June in Minnesota (Figs. 5b,c).

b. Radar morphology

Convection in the experimental domain occurred in three discrete cycles. Each cycle has a distinct line of convective cells that initiate, intensify, and then decay. The first initiated over the Rocky Mountains, the second just east of the foothills, and the third about 100 km east of the Front Range, just outside of the surface mesonet.

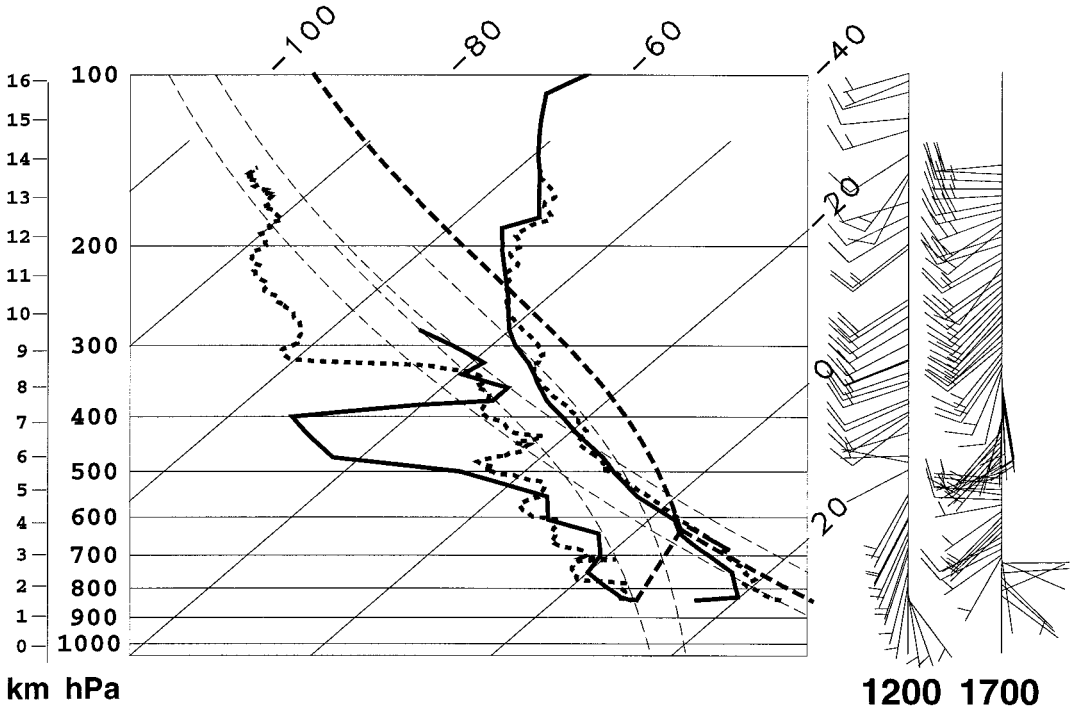

FIG. 4. The Denver skew *T*–log*p* sounding (solid, wind profile A) for 1200 UTC 21 June 1993 and the CLASS sounding (short dashed, profile B) for 1700 UTC. Winds are reported in m s^{-1} (full barb = 5 m s^{-1}). Parcel ascent (long dashed) is based on average conditions near the surface for the CLASS sounding.

Initial convection over the Front Range began at 1730 UTC (1030 MST). Convection between 1000 and 1300 MST along the Front Range is common during the summer months and is typically driven by convergence at ridge top from upslope flow induced by differential surface heating. With the passing short-wave trough providing favorable upper-air conditions, convection became widespread over the mountains. As this line moved eastward over the foothills onto the plains, it encountered a zone where convection is suppressed (Dirks 1969; Tripoli and Cotton 1989). These two studies suggested two possible factors contributing to the suppression of convection at the point where there is a strong change in topographical slope going from the Rockies to the plains: 1) the strong change in the slope of the topography produces an acceleration of the thermally driven slope flow; 2) this is a region of mountain-wave-induced subsidence. The decaying convection produced a strong gust front that propagated eastward from the foothills. Surface convergence between this outflow boundary and the prevailing southeasterlies initiated new convection about 20 km ahead of the decaying line at 1940 UTC. Tripoli and Cotton hypothesized that gravity waves propagating away from the decaying convection may be responsible for the scale selection of where the new convection will initiate.

This new convection (Fig. 6a, cells labeled A, B, and C) was the beginning of the second cycle. At 2000 UTC, 20 min after initiation, four new reflectivity cells had developed to the east of the decaying line. Within 1 h (Fig. 6b), the individual convective cells merged into a convective line approximately 100 km in length. The southern half of the squall line was more homogeneous along its length, while the northern half (where convection developed last) was more cellular. Along the leading edge of the squall line at $y = -35$, -60, and -80 were the beginnings of three small cells. The growth of these new cells was suppressed, as they did not develop beyond what is shown. Thus, the observations indicate that the discrete mode of propagation (of individual convective cells) was suppressed, favoring the longevity of the existing cells and their continuous mode of propagation.

Over the next 2 h the squall line matured, while taking on a characteristic bow-shaped reflectivity pattern (Fig. 6c) similar to the triggering outflow boundary. New growth along the leading edge remained suppressed except right at the northern tip of the line where a new strong reflectivity cell formed. This developed into a line of new convective cells oriented approximately 30° off the northern end of the original line, again 20–40 km ahead of the then decaying second line (Fig. 6d, note the change in scale of the figure).

These new cells were the formative stage of the third cycle. The new line continued to grow and expand southward through new development that formed out ahead of the southern portion of the old squall line. While the newer convection grew, the convection as-

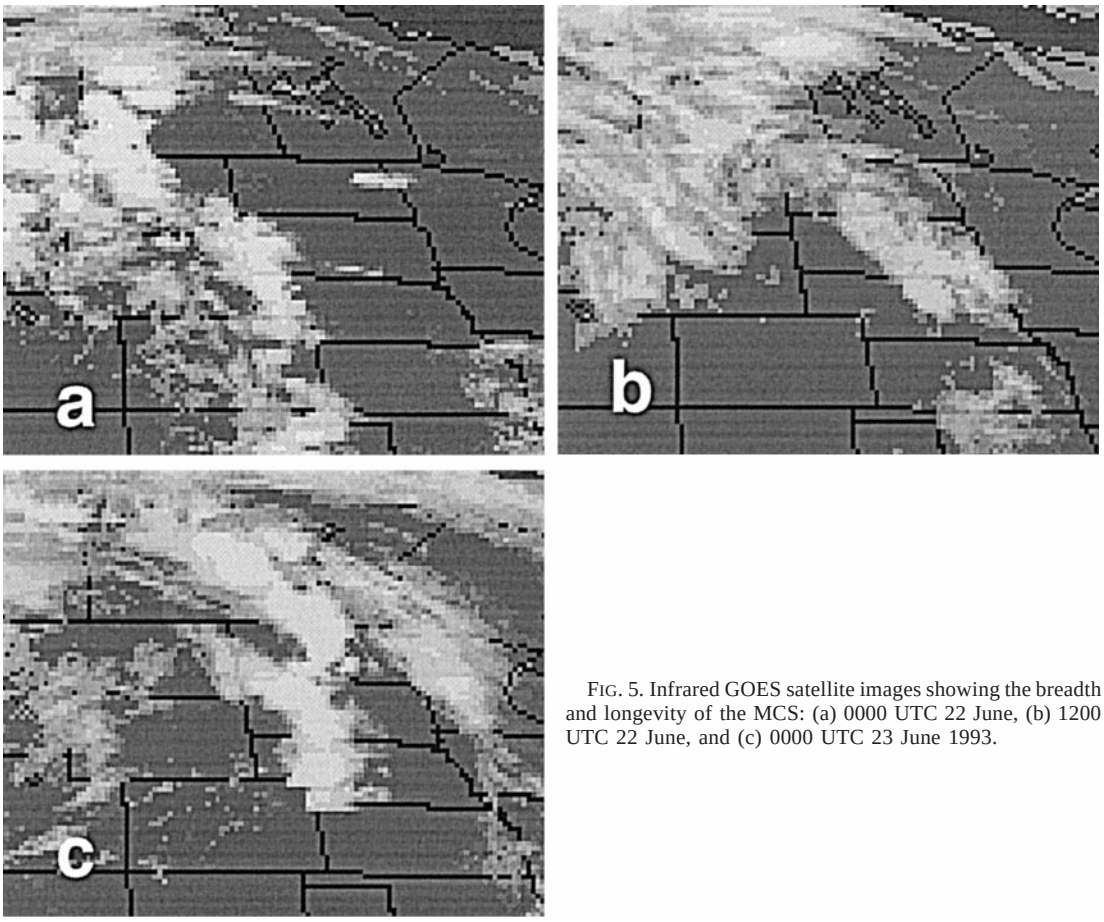

FIG. 5. Infrared GOES satellite images showing the breadth and longevity of the MCS: (a) 0000 UTC 22 June, (b) 1200 UTC 22 June, and (c) 0000 UTC 23 June 1993.

sociated with the original squall line became more stratiform in nature, eventually setting up a precipitation area 60 km in width normal to the line. The convection over the Palmer Divide continued to develop and eventually merged with the stratiform region of the original convective line.

Thus, this squall line propagated with a discrete nature, similar to the 17–18 June 1978 prefrontal squall line, as noted by Matejka [personal communication reported in Cram et al. (1992a)]. Matejka noted that the bigger squall line, which on that day extended from Illinois to the Texas Panhandle, consisted of ''large segments 100 to 200 km long, that marched along in phase, occasionally jumping forward but eventually getting back in step with adjacent segments.'' This description is similar to the evolution of the larger MCS (Fig. 5). Other researchers have observed similar discrete propagation of MCSs, with the discrete ''jump'' distance varying from tens to hundreds of kilometers (Stensrud and Fritsch 1994; McAnelly and Cotton 1986). This mode of propagation is not well understood, but most of the evidence points toward gravity waves as the primary mechanism for initiating convection ahead of the line (Carbone et al. 1990; Tripoli and Cotton 1989; Cram et al. 1992b; Stensrud and Fritsch 1994).

4. Squall line initiation

As the mountain convection propagated eastward over the plain, it decayed. Downdrafts from these storms produced a gustfront that was evident from a fine-line reflectivity pattern in the MHR data at 1915 UTC. At 1937 UTC this fine line was 110 km long and had just passed over the MHR, Stapleton wind profiler/RASS, and PAM station 12 (indicated in Fig. 1). Observations from these platforms were combined to construct a vertical and horizontal picture of the gust front.

A time series from the PAM station 12 revealed a typical gust front signature (Fig. 7). Surface winds turned 180° from prevailing easterlies to westerly, while increasing from 2 to 9 m s^{-1}, when the leading edge of the gust front passed over the station at 1925 UTC. The surface pressure rose, the dewpoint increased, and the temperature decreased from the evaporatively cooled downdrafts created by the decaying convection. After half an hour the temperature and pressure quickly reverted to their undisturbed values as the gust front propagated to the southeast at 6 m s^{-1}.

The RASS afforded a vertical profile of the cold pool. Half-hour averaged virtual potential temperature profiles of the boundary layer just before, during,

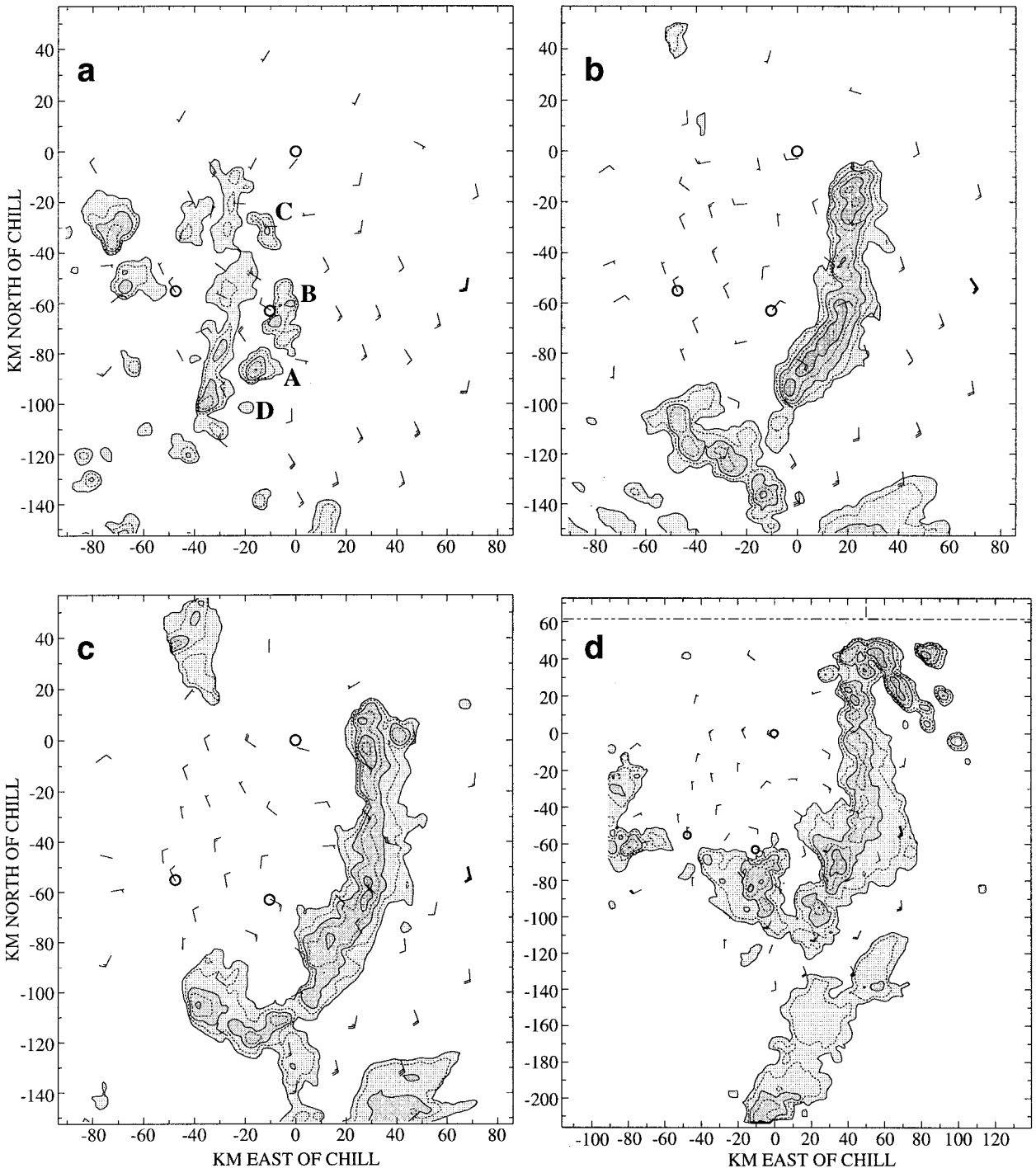

FIG. 6. Constant altitude maps at 3.0 km AGL of the MHR reflectivity fields at (a) 2000, (b) 2100, (c) 2130, and (d) 2200 UTC 21 June 1993. Contours are in 7.5-dBZ increments beginning at 15 dBZ. Shading intervals are 15, 30, and 45 dBZ. Surface winds (full barb = 5 m s^{-1}) from the mesonet are also plotted. Four new cells are labeled A, B, C, and D.

and after the gust front passage (Fig. 8) revealed a 2°C drop in a layer 800-m deep from its second gate at 200 m. The RASS did not observe the temperature drop at the surface. This 2°C temperature drop is small compared to the gust fronts observed by Goff (1974), which exhibited averaged mean perturbations between 2.4° and 6°C.

The RKW conceptual model suggests that the ratio of the strength of the cold pool, c, to the low-level ambient shear, Δu, is a good indicator of the vertical

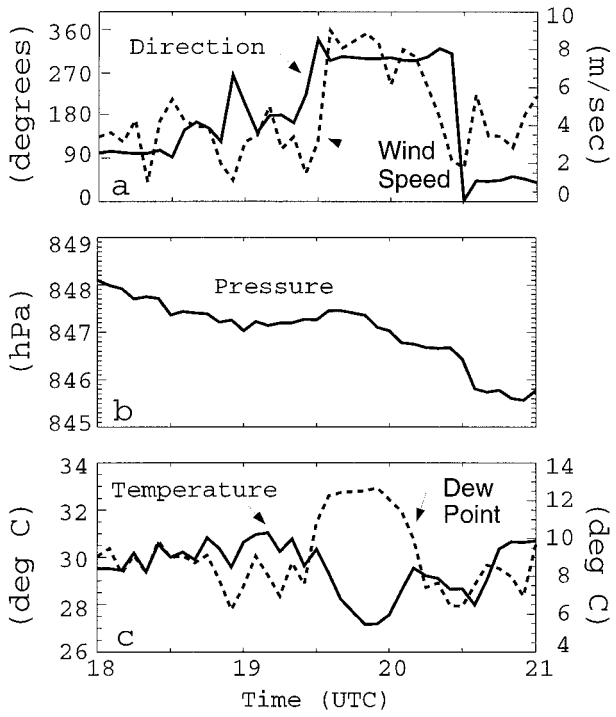

FIG. 7. Time series plot of PAM station 12 data from 1800 to 2100 UTC 21 June 1993. (a) Wind direction (degrees from true north, solid) and wind speed (m s^{-1}, dashed). (b) Station pressure adjusted to 1500 m (hPa, solid). (c) Temperature (°C, solid) and dewpoint (°C, dashed).

orientation of the updraft. Using this ratio, RKW hypothesized that an optimal growth situation and an upright updraft would occur when $c/\Delta u = 1$, a downshear-tilted updraft when $c/\Delta u < 1$, and an upshear-tilted updraft when $c/\Delta u > 1$. They defined the strength of the cold pool c as

$$c^2 = -2g \int_0^H \left(\frac{\theta'}{\overline{\theta}} + 0.61(q_v - \overline{q_v}) - q_c - q_r \right) dz, \quad (1)$$

where θ is the potential temperature; g is the acceleration due to gravity; and q_v, q_c, and q_r are the mixing ratios of water vapor, cloud water, and rainwater, respectively. The overbars and primes represent the unperturbed values and deviations from it, respectively. The integral is calculated through the depth of the cold pool (H) at a representative location behind the leading node of the gust front. While realizing the differences in the physical situations, this ratio was estimated from the observations to determine what this model would predict for this given situation. Since the MHR indicated no precipitation along the gust front between 1915 and 1945 UTC, and any clouds present would be over 2 km above the gust front (from estimated LCL), Eq. (1) becomes (after combining the temperature and vapor effects in the virtual potential temperature, which is the variable measured by the RASS system)

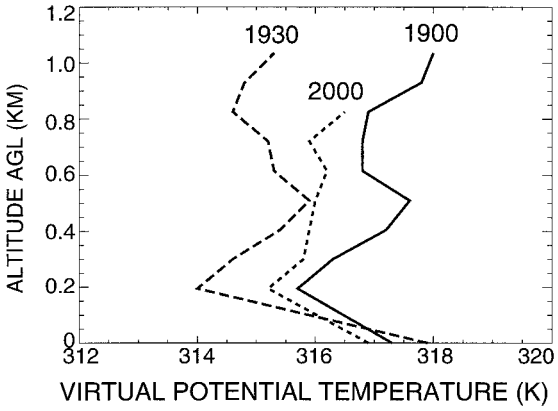

FIG. 8. Time series of virtual potential temperature (K) profiles, calculated from the Denver RASS at 1900, 1930, and 2000 UTC 21 June 1993.

$$c^2 = -2g \int_0^H \left(\frac{\theta_v'}{\overline{\theta_v}} \right) dz, \quad (2)$$

from which c can now be determined from the RASS data to be approximately 11.1 m s^{-1}. The vertical shear of the horizontal wind (determined from the 1700 UTC CLASS sounding) over the same depth is 2.6 m s^{-1}, giving $c/\Delta u \approx 4.3$. Since this value is significantly greater than one, it suggests a more rearward tilted updraft, similar to that observed in the lower troposphere. As predicted, convection initiated 7–10 km behind the gust-front. However, as will be shown in later sections where the updraft evolution is documented, the updraft inside the cloud had a distinctly different tilt.

5. Doppler radar analysis

a. 2017 UTC Doppler analysis

This section summarizes the kinematic structure and associated surface data that are representative of the formative stage of MCS growth. The original four convective cells were still present 35 min after initiation (Fig. 9). The reflectivities to the west of the labeled convective cells were the convection from the first cycle that laid down the outflow boundary and initiated the second cycle's convection. An area of general upward motion was found along the leading edge of the cells with general downward motion on the trailing edge of the reflectivity cells. Embedded within the general upward and downward couplet was an area of maximum upward motion found downshear of cell A with an associated stronger downdraft upshear. The stronger upward and downward velocity couplets were highly correlated with the stronger reflectivity cores. The area of upward motion was initiated by surface convergence along the gust front and was enhanced by midlevel convergence apparent along the leading edge of the 40-dBZ reflectivity cores.

A mean vertical cross section through cell/line A (Fig.

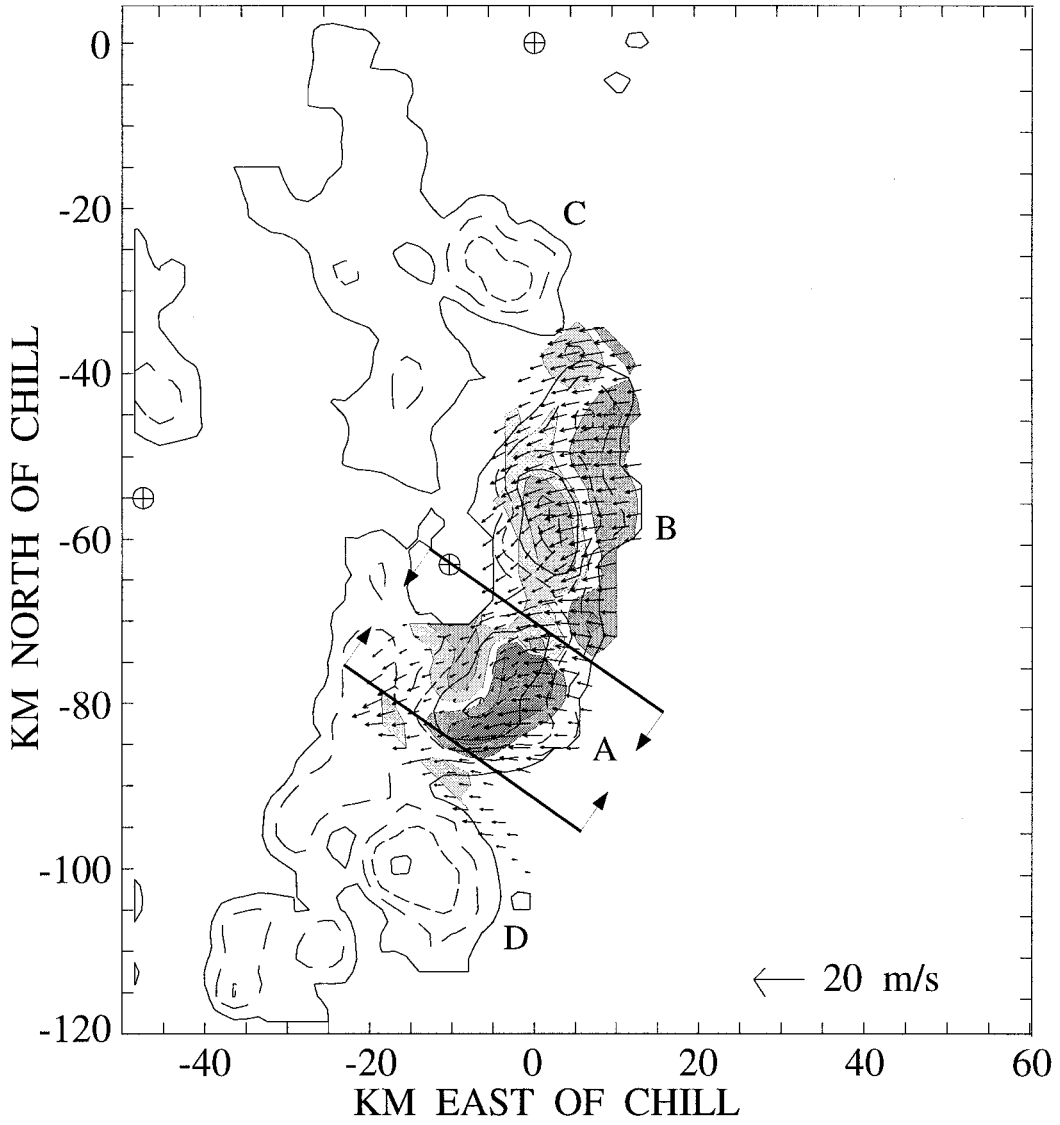

FIG. 9. Triple-Doppler analysis at 3.0 km AGL for 2017 UTC 21 June 1993. MHR contour intervals are in 10-dBZ increments beginning with 10 dBZ. Vectors depict line relative flow. A vector whose length equals one grid interval represents 5 m s^{-1}. Light shading indicate downdrafts; contours are 0 and -2 m s^{-1}. Dark shading indicate updrafts; contours are 2 and 4 m s^{-1}. Reflectivity cells labeled A, B, C, and D are discussed in the text. Heavy lines identify the along-line extend used in developing vertically averaged cross sections.

10) was constructed by along-line averaging over the extent of the 40-dBZ contour at 3 km AGL, as shown in Fig. 9. From this averaged cross section, the updraft tilt was examined. Connecting the centers of the maxima and minima of the horizontal divergence field yielded a similar orientation of the updraft. A rearward-tilted updraft in the lowest 4 km is contrasted to a nearly upright mid- to upper-level updraft. While the rearward tilt of the lower portion of the updraft is in accordance with the hypothesis of RKW, the almost upright updraft in the upper parts is not [see figures in Weisman (1992)]. We attribute this difference to the presence of significant upper-level vertical shear of the horizontal winds.

b. 2102 UTC Doppler and 2100 UTC mesonet analyses

In this section we look at the kinematic structure and associated surface data representative of the intensifying stage of MCS growth. This stage is characterized by the individual cells growing and merging to form a contiguous rain area.

A new cell, E, developed on the northern end of the line at 2020 UTC as cell C started to die. At 2102 UTC (Fig. 11) the original cells, A, B, and D, that the line comprised were about 80 min old, while the newer northern cell E was 42 min old. Cells A and D merged

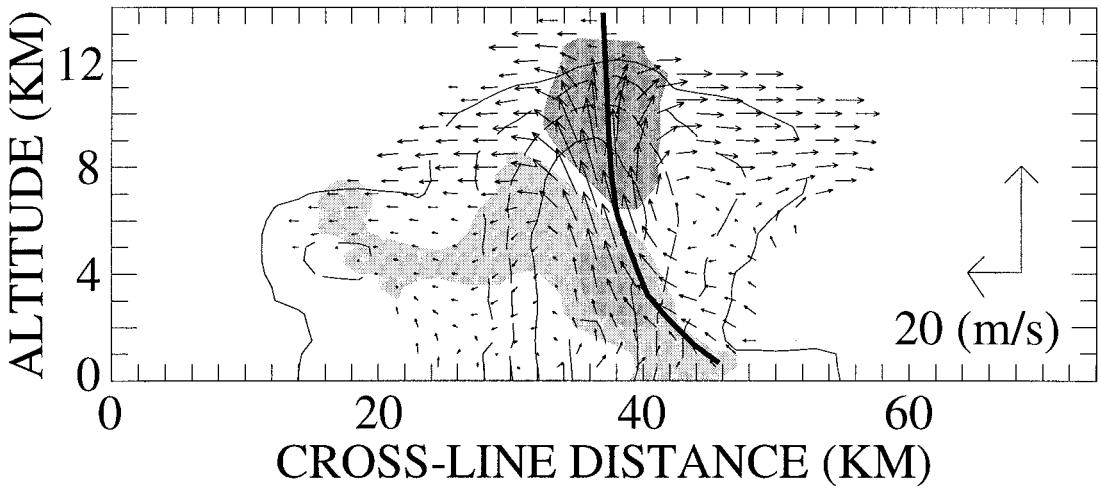

FIG. 10. Along-line averaged cross section through cell A at 2017 UTC 21 June 1993 (see Fig.9). Cross-line distance increases toward the east-southeast. Reflectivity contours are in 10-dBZ increments beginning with 10 dBZ. Vectors depict line relative flow. Light shading indicates convergence, contours are 0 and -10^{-4} s^{-1}. Dark shading indicates divergence; contours are 10^{-4} and 2×10^{-4} s^{-1}. The dark line represents the axis of maximum updraft speeds.

approximately 15 min prior to this time and henceforth are labeled A and referred to in the text as line A (Fig. 11). Midlevel convergence along the entire leading edge of the line enhanced the preexisting upward vertical velocities created by surface convergence, though stronger areas of upward and downward motion were still positively correlated to the reflectivity cores.

Orientation of the updraft and downdraft couplets with respect to the reflectivity cores along the length of the line varied between the northern and southern parts of the line. To the south, where the line was oriented about 30° clockwise from the north, the velocity couplet was on the leading and back edge of the reflectivity core. The northern cells that were oriented in a north/south line had the updraft farther ahead of the reflectivity core with the downdrafts collocated with the reflectivity core. Midlevel rear-to-front flow was prevalent throughout the back of the southern line A but was not seen on the back of the northern cell E. Rather, strong descending front-to-rear flow with an associated surface fine-line reflectivity feature (not shown) was observed behind cell E.

The along-line averaged cross section for the southern part of the line in Fig. 12a showed the vertical structure at the intensifying stage. A maximum average vertical velocity of 9.6 m s^{-1} was attained in the updraft with a localized maximum of 17.5 m s^{-1}. The midlevel convergence and upper-level divergence maximums had not changed much in position from the previous analysis. However, the low-level convergence center moved slightly farther downshear from the convective core associated with the movement of the gust front. As in the previous analysis (see Fig. 10), the reflectivity core again tilted slightly forward. The upper-level anvil was well developed, with a preference in growth to the front. The anvil on the trailing anvil was 28 km wide, while the leading anvil was 33 km wide. Indications of an organized rear inflow can be seen at the base of the anvil just behind the reflectivity core. A small averaged area with rear-to-front flow greater than 5 m s^{-1} existed while the maximum localized speed was 8.8 m s^{-1}. Studying rear inflow within the stratiform region of squall lines, Smull and Houze (1987b) classified rear inflows as moderate for magnitudes between 5 and 10 m s^{-1}. As observed with Ogura and Liou (1980) for the mature stage of a midlatitude squall line, this intensifying stage also showed a nearly conservative band of *u*-momentum front-to-rear flow with stronger flow at the rear of the upshear anvil.

Comparing the along-line averaged cross section of line A (Fig. 12a) with cell E (Fig. 12b) at the same point in its growth yielded some striking differences. Cell E showed a distinct leading anvil with descending midlevel front-to-rear inflow at the bottom of the anvil, extending almost the entire length of the 40-km anvil. A broad, gradual updraft led into the 25-dBZ reflectivity core for cell E, in contrast to a narrow, more pronounced updraft for line A. The differences will be further discussed later in this paper.

At 2100 UTC, a well-defined mesohigh was located beneath the line of convection (Fig. 13). A broad region of higher pressure was also located in front of the convection under the leading anvil. Warm south-southeasterly winds ahead of the squall line suggested that the gust front had not propagated well ahead of the convection and, therefore, was not the cause of the higher pressure under the leading anvil. Three troughs existed: one being the gust front along the leading edge of the convection, another located behind the storm in a wake-low position (Johnson and Hamilton 1988), and a third located farther ahead of the gust front trough.

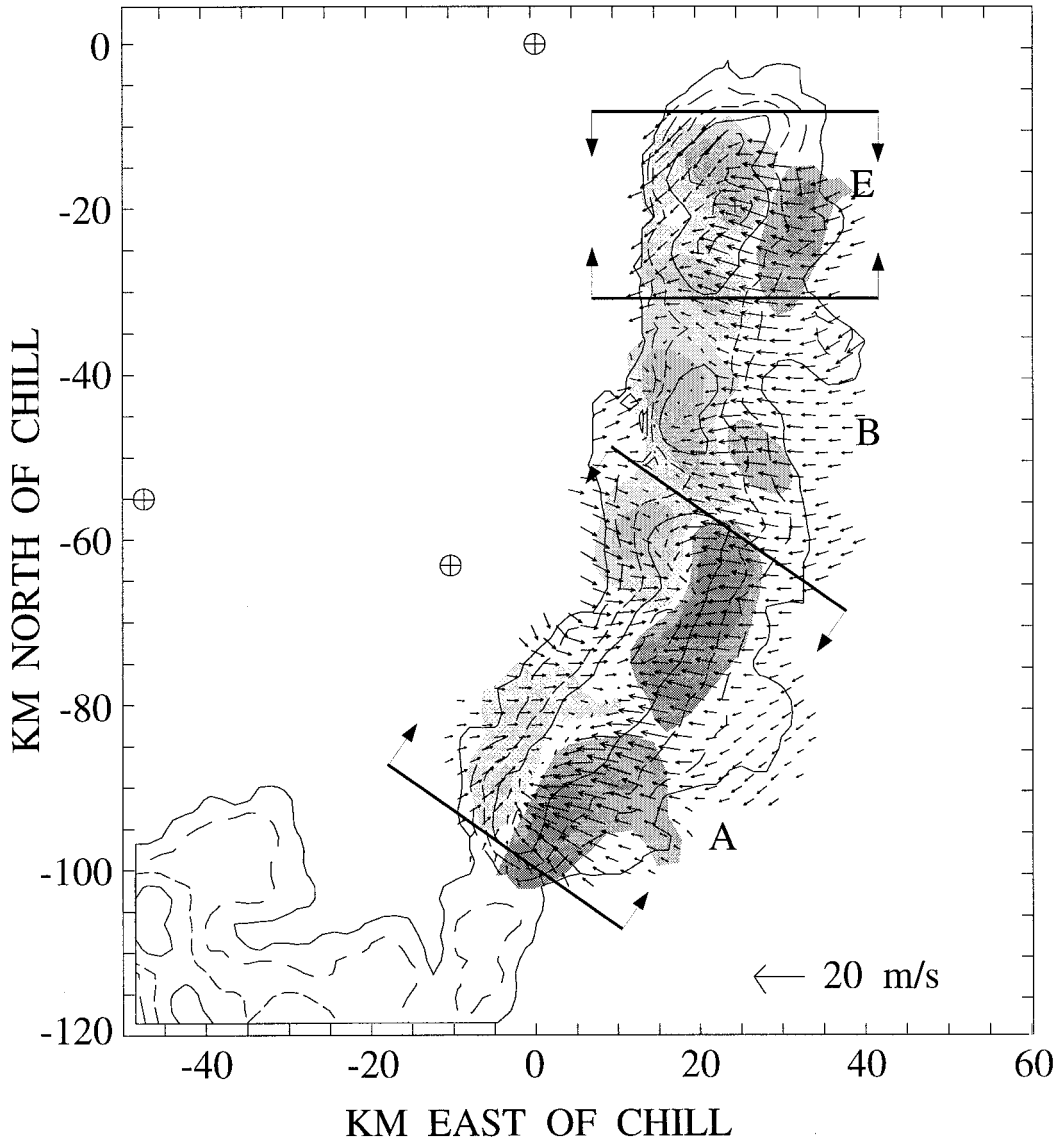

FIG. 11. As in Fig. 9 except for 2102 UTC 21 June 1993.

Speed convergence was evident across the leading trough.

c. *Vertical profiles of kinematic fields*

Further insight into the development of the squall line and the differences between the southern and northern ends are ascertained through a time series of vertical profiles. Mean vertical profiles of the horizontal divergence in cell/line A (Fig. 14) for the first six analysis times were constructed by averaging over the entire cross-line extent of the >40 dBZ region at 3 km as indicated in Fig. 10. At the surface, weak divergence generally strengthened in time, suggesting an increasing influence from evaporatively cooled downdrafts. Convergence at midlevels dominated with progressively increasing strength over time. Also noted was an increased depth to the midlevel convergence with the level of nondivergence (LND) stopping at about 6 km in the final analysis. Near storm top, divergence quickly peaked, then weakened for about 45 minutes, strengthened again, then finally weakened to a temporal minimum. Associated with these divergence profiles are a series of maximum upward velocities (Fig. 15). Similar pulsating behavior of the updraft has been modeled by several groups (e.g., Crook and Moncrief 1988; Weisman et al. 1988; Tripoli and Cotton 1989; Fovell and Dailey 1995) and has been attributed to different causes. In the Weisman et al. (1988) simulation, different maxima correspond to individual cells initiating, maturing, and decaying in succession, while Tripoli and Cotton (1989) attributed the pulses to a self-modulating gravity

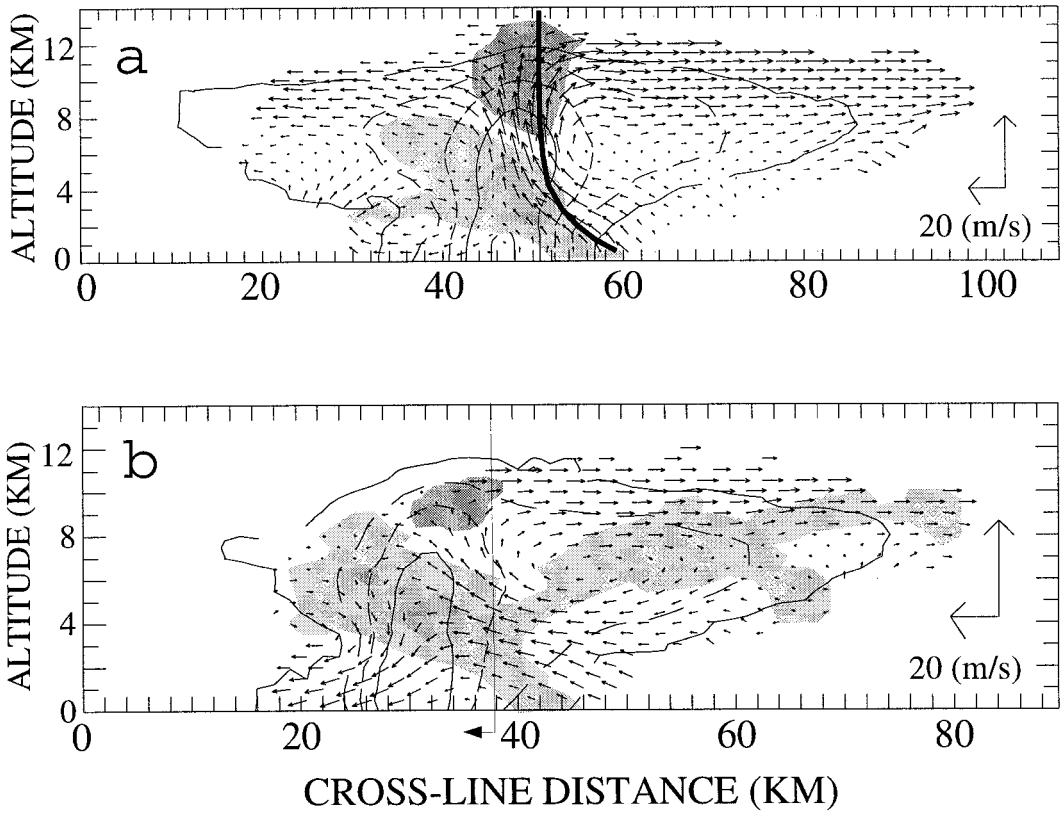

FIG. 12. As in Fig. 10 except for (a) line A at 2102 UTC and (b) cell E at 2131 UTC 21 June 1993 (see Fig. 11). These represent similar stages of development for the two line segments. In (b) distance increases toward the east; to the left of the line in (b) the vertical component of the wind is unreliable.

wave mechanism. Fovell and Dailey (1995) found that the periodicity is related to the strength and the depth of the environmental shear. The second peak in the vertical velocities in Fig. 15 corresponds to a period after the system propagated into a region of slightly higher θ_e air, with its front-to-rear midlevel inflow becoming organized, (Fig. 16, discussion following). Therefore, it is possible that the increase in vertical velocities are a result of more energy rich boundary layer air, rather than a storm dynamic argument.

Vertical profiles of line-normal horizontal wind averages in a box 2 km wide, centered approximately 10 km ahead and behind the convective cores of the previously defined line segments, were constructed to further categorize the flow around the MCS. The boxes were advected with the storm to show the evolution of the flow at approximately the same location relative to the storm. This was done separately for the southern and northern sections of the line.

Figure 16 shows the results for the southern section. The back of the squall line showed an increasing surface outflow at low levels. On the front, there was no clear indication that the gust front leading the squall line propagated away from the storm. With the strengthening outflow at the surface, the increasing midlevel convergence (see Fig. 14) provided mass for downdrafts and correlated well with the surface divergence. At midlevels, an increased rear inflow was readily apparent on the back. The maximum winds were generally found at about 3.5 km with a magnitude of 4.7 m s^{-1}. On the front side of the squall line the storm relative inflow increased, while the maximum winds were found lower (at 2.5 km) and stronger (at 7.7 m s^{-1}) than the back side of convection. Vertical cross sections of low-level flow showed the low-level updraft becoming more tilted with time. Near storm top on the back side, the line-normal front-to-rear velocities remained nearly uniform in structure and speed. The maximum flow in the upshear anvil at the 9-km level was 8.5 m s^{-1}. The front side did experience fluctuations that account for the differing divergence strengths aloft (see Fig. 14). Most of the change in upper-level divergence was attributed to flow ahead of the line. The magnitude of the flow in the leading anvil varied between 10.0 to 18.5 m s^{-1}. When upper-level divergence and upward velocities were maximized, the flow in the leading anvil was between 130% and 145% larger than that of the flow in the trailing anvil.

Differences in the divergence profiles of cell/line A and cell E can be seen in Figs. 14 and 17. Maximum midlevel convergence for cell E was about 100% greater than the maximum for cell/line A. Also, the LND was

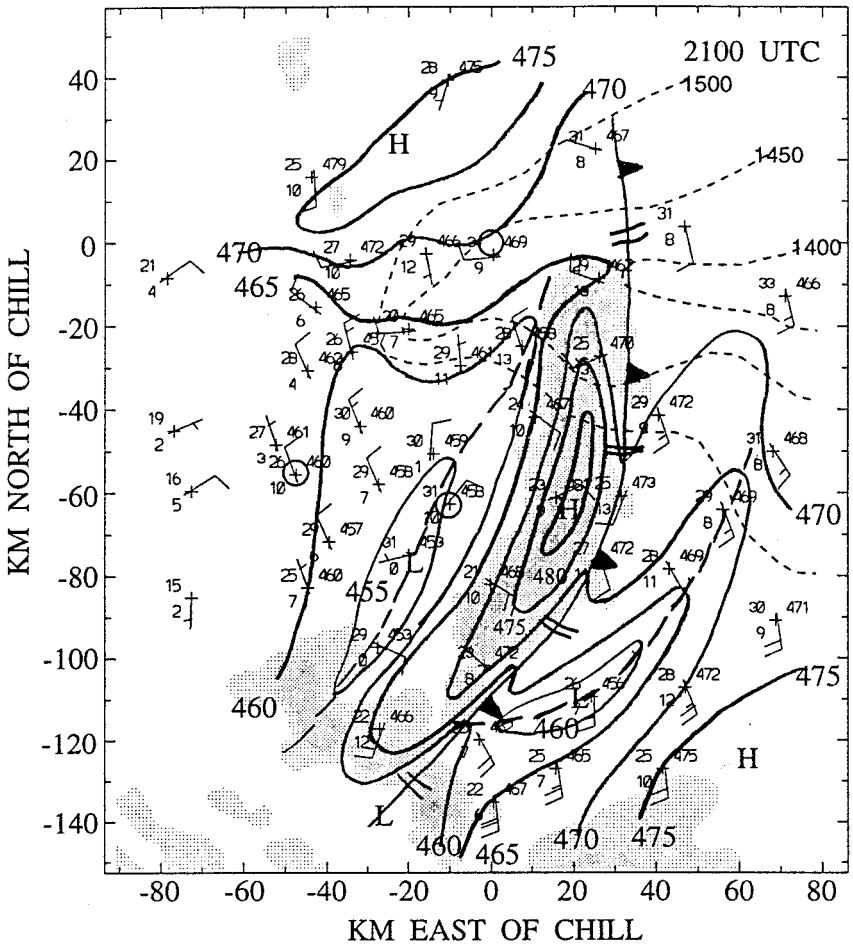

FIG. 13. Mesonet surface analysis for 2100 UTC 21 June 1993. Same plotting convention as in Fig 3. Station pressure is contoured at 0.5-hPa intervals (solid). MHR reflectivity at 3.0 km AGL superposed with shading contours at 15-, 30-, and 45-dBZ levels. Dashed line represents the terrain contours for 1400, 1450, and 1500 m.

located approximately 1 km higher for much of the analysis time as compared to the maximum height for any of the analysis times for cell/line A. The height of the maximum in the convergence was approximately 4 km, which was also 1 km higher than cell/line A. The upper-level divergence location and strength were believed to be suspect above 9 km, caused in part by the storm top being unresolved as a result of the low maximum scan height by the CSU-CHILL radar.

Plots of winds on the front and back of cell E, Fig. 18, were calculated in a similar fashion as Fig. 16. Winds on the back side of the storm in Fig. 18a exhibit the greatest variability of all of the vertical wind profiles. Winds were generally front-to-rear below 4 km and rear-to-front above 4 km. The horizontal wind profile for the front side (Fig. 18b) was much more consistent than the backside, and looked very similar to the profile for the cell/line A (see Fig. 16b), except that the inflow was deeper and stronger. Surface flow on the front did experience an increased strength to the point where the flow was moving away from the MCS. This flow suggested that the gust front may have started moving away from the squall line. At midlevels up to 4.5 km, stronger rearward flow on the front than the back caused speed convergence. From 4.5 to 6.5 km, the midlevel convergence became a combination of both speed and directional convergence. At upper levels, speed divergence existed due to stronger leading flow along the front than along the back. Above 8.0 km on the backside of the cell, there was little to no flow rearward, which agreed with the lack of a trailing anvil.

A time series of the updraft tilt is shown in Fig. 19. The tilt was objectively determined by connecting the maxima of surface convergence, midlevel convergence, and upper-level divergence. This method correlates well with the axis of maximum upward motion as seen in Figs. 10 and 12a. For the southern cell/line A (Fig. 19a), the only tilt to the updraft was from low to midlevels, primarily below cloud base. This tilt is associated with the gust front being ahead of the convective line. From

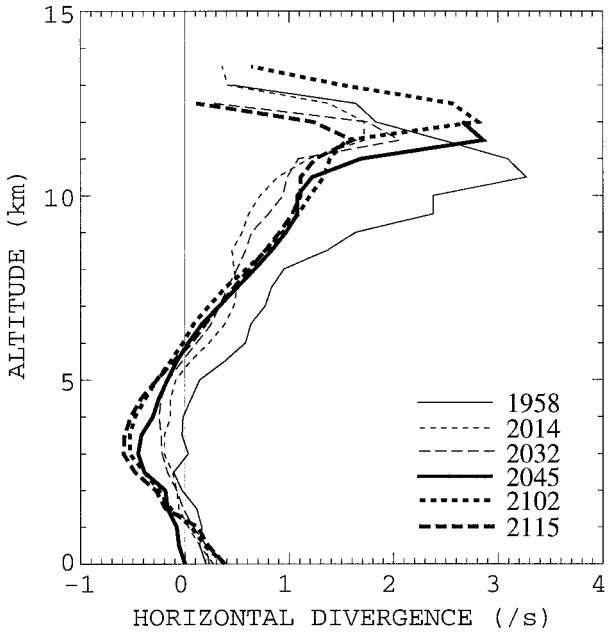

FIG. 14. Time series of horizontal divergence profiles ($\times 10^{-4}$ s^{-1}) calculated for cell/line A for times 1958 through 2115 UTC 21 June 1993.

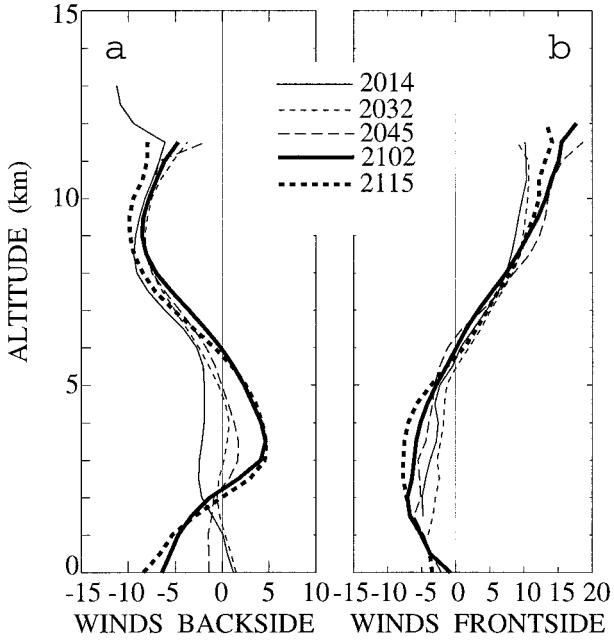

FIG. 16. Time series of profiles of averaged storm-relative, line-normal wind components (m s^{-1}) calculated for cell/line A in the (a) back and (b) front of the main convective line for the times 2014 UTC through 2115 UTC 21 June 1993. Domain used for the averaging was located approximately 10 km behind and ahead of the main convective line and was advected with the storm to yield winds representative of the same approximate location within the storm.

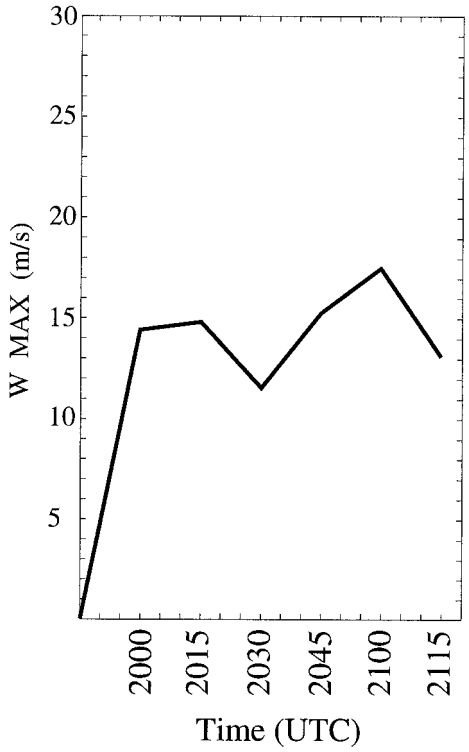

FIG. 15. Temporal variation of observed vertical velocities for cell/line A.

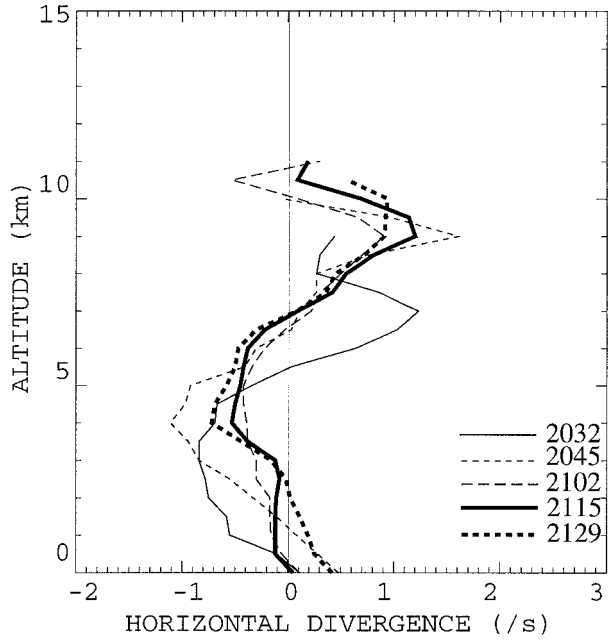

FIG. 17. Time series of horizontal divergence profiles ($\times 10^{-4}$ s^{-1}) calculated for cell E for times 2032 through 2129 UTC 21 June 1993.

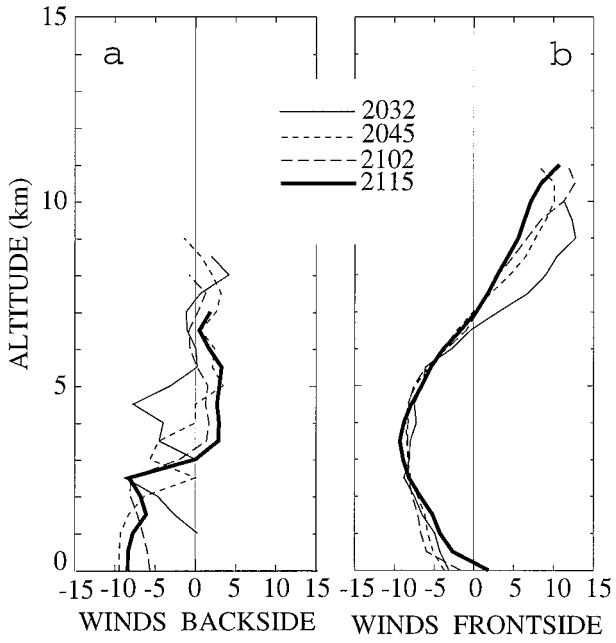

FIG. 18. Time series of profiles of averaged storm-relative, line-normal wind components (m s^{-1}) calculated for cell E in the (a) back and (b) front of the main convective line for the times 2032 UTC through 2115 UTC 21 June 1993. The same procedure was used to determine the wind profiles as in Fig. 16.

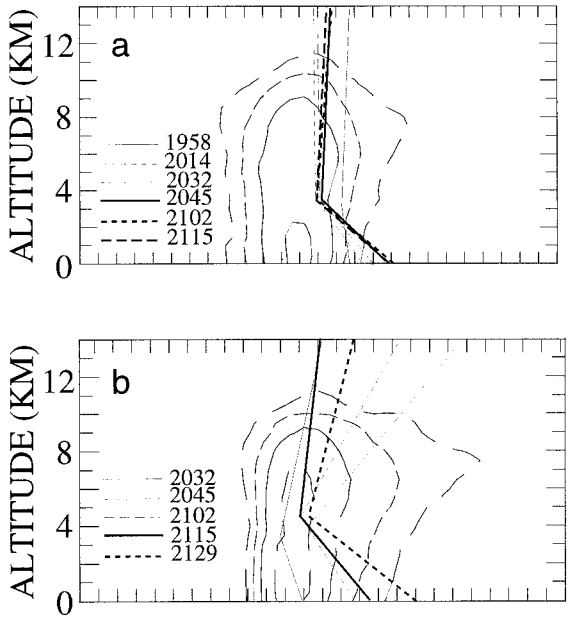

FIG. 19. Time series of updraft tilt calculated for (a) cell/line A and (b) cell E for times indicated in the legends for 21 June 1993. The updraft tilt was objectively determined by connecting the maxima of the surface and midlevel convergence and upper-level divergence. Representative reflectivities are at 2017 for cell A and 2045 for cell E. Reflectivities are contoured at 10 dBZ intervals starting at 20 dBZ.

middle to upper levels within the storm, a nearly upright updraft existed throughout the analyses. For the northern cell E (Fig. 19b), the low to middle levels again show the strongly tilted updraft. The location of the upper-level divergence maxima tended first to move downshear (through 2102), then rearward with time. This factor is attributed to the unresolved storm top. By the last analysis the divergence location was considered to be more representative of the true situation, as more of the storm top was resolved after moving farther away from the CSU-CHILL radar. This last analysis showed a forward tilt from mid to upper levels, in contrast to the upright structure of the southern end.

Asymmetries between cell/line A and cell E persisted throughout the analyses. The asymmetries identified in this section included the differing location of the anvil and rear-inflow jet, updraft orientation and structure, divergence, and wind profiles. As discussed in the next section, these differences are attributed to observed environmental inhomogeneities.

6. Discussion

RKW concluded in their study that the nonsupercellular squall line may be viewed as a long-lived line of ordinary short-lived cells. They further suggested that most of the squall line's structural features and its longevity result from the interaction of the storm cell's cold surface outflow with the low-level shear. The 21 June 1993 squall line exhibited many characteristics that did not fit this model. Similarly, the 21 June event did not fit the WKR simulation. In particular, WKR presented model results for low-level vertical wind shear of 10 m s^{-1} through 2.5 km and 5.0 km AGL (WKR, see Figs. 5 and 15, respectively) conditions that are close to the 21 June observed 8 m s^{-1} shear over similar levels. When the WKR simulations are compared to both of the along-line averaged vertical cross sections for the northern and southern ends, many differences are evident (Table 1).

These modeling studies focused on the impact of the

TABLE 1. Comparisons between the WKR numerical simulations using vertical wind shear of 10 m s^{-1} over 2.5 and 5.0 km and the observations between cell E on the northern end of the squall line and cell/line A on the southern end.

	Conceptual model	Observed	
		north	south
Upshear tilted updraft throughout the depth of the troposphere	yes	NA	no
Predominantly upshear anvil	yes	no	no
Propagation of squall line through a typical multicelled fashion	yes	no*	no
Rear-inflow jet	no	no	yes
Descending front-inflow jet below the leading anvil	no	yes	no

* Initial multicellular propagation soon gave way to the more discrete jump as the new line developed southeastward.

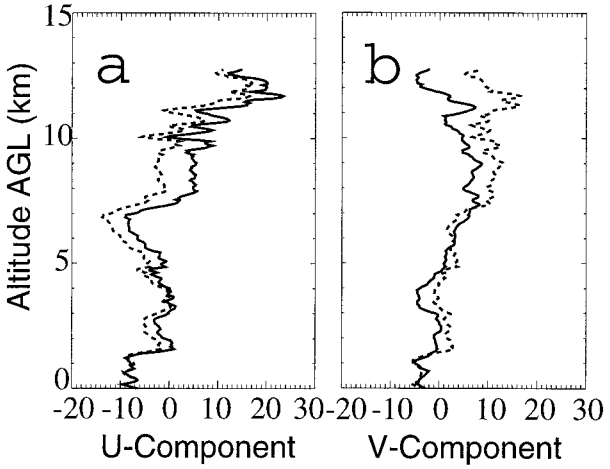

FIG. 20. Line-relative ambient wind profiles of (a) line-normal and (b) line-parallel for cell E (oriented north–south, solid) and cell/line A (oriented north-northeast–south-southwest, dashed) as determined from the 1700 UTC CLASS sounding.

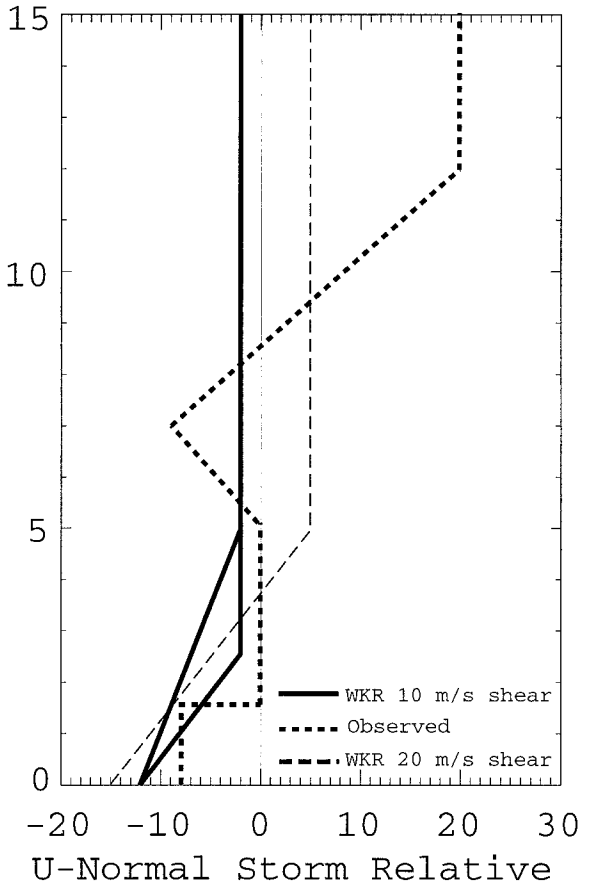

FIG. 21. Wind profile of the line-normal component of the wind relative to storm motion. Cases plotted are indicated in the legend.

interaction between the surface outflow and the low-level shear on the storm; however, other factors that may impact storm structure and longevity were not investigated. The 21 June storm did not evolve as a line of ordinary short-lived cells. Rather, long-lived individual cells in the line existed for more than three hours, while new convection along the leading edge of the gust front was suppressed. Factors that may have impacted this storm are the large-scale forcing associated with a passing short-wave trough, the environmental wind shear profile, and inhomogeneities in the environment through which this storm propagated. Crook and Moncrieff (1988) suggested that when large-scale forcing exists, lifting at the cold pool is not critical in maintaining the convective system. It is clear that there exists a broader range of structures of squall lines than presented by the RKW theory and that a fuller understanding of this variety will require much more modeling work involving a wider variety of initial conditions.

a. Impacts of shear

In the numerical modeling work of Thorpe et al. (1982), RKW, and WKR, moderate shear confined to the lower 2.5 km with constant winds above was determined as optimal to the strongest and longest-lived convective systems. By varying the shear profile alone, a wide range of observed squall line structures and longevities were simulated. Figures 20a,b shows the shear profile relative to the line (using the 1700 UTC sounding) for both the northern and southern ends. Low-level shear was less than 10 m s^{-1} and confined primarily to a shallow layer at 1.5 km with essentially no shear through the depth later replaced by the cold pool. However, unlike the modeling profiles used, there was significant shear higher in the troposphere (10 m s^{-1} rearward shear between 5 and 7 km, and 30 m s^{-1} forward shear between 7 and 12 km). The strong upper-level shear is more like the case observed and modeled by Schmidt and Cotton (1989, 1990), and observational study of Nachamkin et al. (1994). Schmidt and Cotton found that strong upper-level shear was necessary to produce a long-lived squall line in their simulations. The strong upper-level shear produced the predominantly leading anvil in the 21 June case. The vertical transport of low momentum low-level air by the convective updrafts produces a high pressure region on the upshear side of convective cores (Cotton and Anthes 1989, p 425; Nachamkin et al. 1994). The downshear-directed perturbation pressure gradient force then accelerates the air downstream, producing the leading anvil (Schmidt and Cotton 1990; WKR).

Figure 21 shows the environmental winds relative to storm motion for the three WKR simulations and the observed 21 June squall line. At low levels westward motion was present for all cases, decreasing in strength with height for the three modeling cases. However, in the observed case there was no shear in the lower 1.5 km. The modeling studies emphasized that moderate to strong Δu between the surface and the top of the gust front is necessary for squall line longevity. Using the

gust front depth as observed by the RASS system as characteristic for this system, Δu was only $\sim$2.6 on 21 June. Therefore, other mechanisms had to be at work. We hypothesize that the horizontal vorticity inherent in the upper-level shear counteracted the tendency to tilt rearward, resulting in an upright system. This configuration, a strongly tilted low-level updraft becoming more upright higher in the cloud, allowed the individual convective cells to persist for long periods while propagating in a continuous fashion.

Bluestein and Jain (1985) in their further discussion section ask, ''. . . and since there is a systematic relation between squall line orientation and the vertical shear, could it be that the relative orientation of the surface boundary to the vertical shear is an important factor?'' This appears to be true for this case. In Fig. 20a, the northern end of the line, which was oriented in a north–south direction, shows a stronger cross-line flow than the south end. But in Fig. 20b, the southern end, which was oriented more northeast–southwest, shows a stronger alongline flow than the north. This does indicate that the orientation of the line could indeed have had an impact on the structure of the squall line, and hence its evolution and observed asymmetries.

b. Impacts of thermodynamics

Like vertical shear, variations in thermodynamics and topography complicated comparisons to the WKR conceptual model and may have also contributed to the observed asymmetries along the line. Thermodynamic properties of the environment vary widely in time and space. As noted previously, all of the RKW, WKR, and Weisman (1992) simulations used a representative sounding in a homogeneous environment for model initiation. Compared to the 21 June prestorm sounding, their sounding has a low LFC of 1.7 km (vs 3.1 km). In the numerical simulations that yielded optimal squall line development, the cold pool that developed was between 1.7 and 2.5 km deep (Weisman 1992, see his Fig. 2). With an LFC of 1.7 km, convection starts along the leading edge of the gust front, which allows the circulation created from the horizontal buoyancy gradients to enhance the updraft initiated from surface convergence. However, in this case convection did not initiate along the leading edge of the gust front, but rather, due to a shallow cold pool and high LFC, was initiated 7–10 km behind the leading edge of the gust front. In addition, Crook (1996) found that the shear layer above the top of the cold pool inhibited convective initiation along the gust front. These differences in the thermodynamic structure of the atmosphere have significant influences on the development of the squall line.

The updrafts in the mid- to upper levels of the line remained upright to slightly forward tilted throughout the period of observations (Fig. 19). This tilt is in contrast to the strong rearward tilt predicted by the WKR criteria based on the environmental shear and cold pool conditions. Therefore, it is hypothesized that the location of the convection 10 km behind the leading edge of the gust front and the height of the LFC minimized the impact of the cold-pool-induced circulation at cloud base. Once the rising airmass reached the LFC it became more positively buoyant and accelerated upward. As it did so, it increasingly felt the impact of the upper-level shear and became more erect. Thus, the structure was not as much determined by the lower-level cold pool–ambient shear interaction but more by the shear profile of the entire atmosphere.

c. Propagation mode

Although new cells initiated along the downshear side of the southern portions of the squall line, these cells did not develop like the cells to the north did. This suppression of convection could be the result of a variety of factors. Tripoli and Cotton (1989), in a modeling study in the same geographical area, found that the mountain slope flow acts to nurture and strengthen the plains inversion, which would limit the initiation of new convection. In another numerical study, Stensrud et al. (1991) found substantial cooling rates in the subanvil region associated with sublimation, evaporation, and melting. In the southern parts of the line, new convection developed below the downward branch of the strong convective overturning (see Fig. 10). Sun et al. (1993) have found that these downdrafts just ahead of the main convective updrafts consist of air forced below its equilibrium level, and thus are warmer than the environment. This, in association with the strong cooling rates (below the anvil area) found by Stensrud et al., would tend to stabilize a region just below the downdraft area where the new convection in the south developed. Alternatively, it is possible that the shear just above the boundary layer (Fig. 20) may have inhibited the formation of strong convection in the absence of additional forcing (Crook 1996). The dataset does not contain sufficient information to give a definitive answer.

At about 2230 UTC the gust front strengthened as the descending rear-inflow jet, in combination with the decay of the second cycle convective cells, produced strong outflows (observed in the mesonet). This intensified gust front had propagated into an environment more favorable for convective development. Tripoli and Cotton (1989) and Stensrud and Fritsch (1994) have hypothesized that gravity waves propagating away from the convection may be responsible for creating favored areas for convective initiation. These, in association with the strengthening gust front and convergence into the trough ahead of the squall line (see Fig. 13), are hypothesized to be the cause of the new convection that formed within 1 h approximately 40 km out ahead of the old convective line. Unfortunately, no observational evidence was found to support this hypothesis, other than the initiation of the convection ahead of the line. At this point, the original convective cells and

line along the southern portion of the squall line were almost 3 h old.

Along the northern end of the squall line the line-normal winds were stronger (Fig. 20a). As a result, the downward branch of the overturning gyre was farther downstream (Fig. 12b), allowing new convection to develop closer to the original reflectivity cells.

Thus, the northern section of the line propagated through what appeared to be a discrete mode of propagation of individual cells. In contrast, the southern section of the line propagated discretely through the initiation of new convection some distance ahead of the existing line. Individual cells in the southern section were longer lived and appeared to be propagating in a more continuous fashion.

7. Conclusions

The conceptual model advanced by RKW and WKR suggested that the observed features of squall lines could be explained through a balance between the circulations induced by the low-level ambient vertical shear of the horizontal wind ahead of the line and that induced by the horizontal buoyancy gradient along the leading edge of the convectively generated cold pool. These circulations dictated the orientation of the updraft, which was key to understanding the structure and longevity of squall lines. This model has contributed significantly to our understanding of the impact of low-level shear on squall line structure. However, squall lines exhibit a broad range of structures, many of which cannot be explained by this model. To obtain a fuller understanding of the variety of observed squall line structures it is necessary to do more modeling work, involving a greater variety of different conditions. Observations in this study indicated that the large-scale forcing, upper-level shear, cloud base height, topography, and atmospheric stability profile also contributed to the structure and mode of propagation.

In this case, the drier thermodynamic profile resulted in convection forming not along the leading edge of the gust front, but rather 7–10 km behind the leading edge and approximately 1.8 km above the top of the cold pool. The preconvection atmospheric shear profile indicated little shear through the depth of the cold pool, but had strong shear in a shallow layer above the boundary layer and also in the upper atmosphere. The squall line exhibited a strongly rearward-tilted updraft in the lower atmosphere, which became more erect in middle levels and was almost erect from the middle- to the upper-troposphere, indicative of the impacts of both the lower-level as well as the upper-level shear profiles.

Strong upper-level shear was significant to the establishment of a leading anvil. This upper-level shear positioned the downward branch of the convective overturning at the tropopause toward the front of the squall line, where it was hypothesized that it contributed to the suppression of the discrete mode of propagation of individual cells in the southern parts of the line. Individual cells persisted for more than 3 h. After the line matured and a rear-inflow jet developed, new convection was initiated about 40 km ahead of the original line, reminiscent of the descriptions of the 17–18 June squall line by Matejka (Cram et al. 1992a). Along the northern part of the line, which was aligned differently toward the shear, individual cells propagated discretely.

This case illustrates the need for additional study into factors impacting the structure, evolution, and propagation of squall lines. Influences of local inhomogeneities, and spatial and temporal variations in the environment need to be determined. Recent work by Skamarock et al. (1994) has begun to address these inhomogeneities. More actual case studies are needed, rather than additional work in idealized environments, so that other important modulators of the squall line characteristics may be found. The 21 June squall line developed in an environment in which, according to the dominant theory of squall line development, it should not have persisted as long as it did. Specific questions that need to be answered are: 1) What is(are) the mechanism(s) that leads to the discrete propagation that has been observed in this study and others? 2) What is the sensitivity of storm structure to irregular shear/thermodynamic profiles? This is in addition to just varying the 2.5-km shear strength and/or the depth of the shear. The atmosphere seldom produces the smooth shear profiles frequently used in models. The observations described in this paper and the modeling work of Crook (1996) indicate that little quirks in the profiles (such as the low-level shear primarily contained in a shallow layer above the cold pool depth) may have a significant impact on the storm structure.

Acknowledgments. The first author was supported by the U.S. Air Force and Air Force Institute of Technology (AFIT) Civilian Institution Program. Mike Fritsch provided valuable input. We thank Ray McAnelly, Andrew Crook, and one anonymous reviewer for their thorough reviews of this paper. Data were provided by Kultegin Aydin (PSU), Bob Rilling and Peter Neilley (NCAR/ATD), Tom Ross (NCDC), and Dave Merritt (NOAA/ERL). Michele Case, Jay Miller, and Bill Anderson (NCAR) provided help with the analysis software, and Paul Hein and Jason Nachamkin provided plotting packages that have allowed this project to be presentable. The satellite images were provided by WSI.

REFERENCES

Bluestein, H. B., and M. H. Jain, 1985: The formation of mesoscale lines of precipitation: Severe squall lines in Oklahoma during the spring. *J. Atmos. Sci.*, **42,** 1711–1732.

——, G. T. Marx, and M. H. Jain, 1987: Formation of mesoscale lines of precipitation: Nonsevere squall lines in Oklahoma during the spring. *Mon. Wea. Rev.*, **115,** 2719–2727.

Browning, K. A., and F. H. Ludlam, 1962: Air flow in convective storms. *Quart. J. Roy. Meteor. Soc.*, **88,** 117–135.

Cahir, J. J., J. M. Norman, and D. A. Lowry, 1981: Use of a real-time computer graphics system in analysis and forecasting. *Mon. Wea. Rev.,* **109,** 485–500.

Carbone, R. E., J. W. Conway, N. A. Crook, and M. W. Moncrieff, 1990: The generation and propagation of a nocturnal squall line. Part I: Observations and implications for mesoscale predictability. *Mon. Wea. Rev.,* **118,** 26–49.

Cotton, W. R., and R. A. Anthes, 1989: *Storm and Cloud Dynamics,* p. 425. Academic Press, 883 pp.

Cram, J. M., R. A. Pielke, and W. R. Cotton, 1992a: Numerical simulation and analysis of a prefrontal squall line. Part I: Observations and basic simulation results. *J. Atmos. Sci.,* **49,** 189–208.

——, ——, and ——, 1992b: Numerical simulation and analysis of a prefrontal squall line. Part II: Propagation of the squall line as an internal gravity wave. *J. Atmos. Sci.,* **49,** 209–225.

Crook, N. A., 1996: Sensitivity of moist convection forced by boundary layer processes to low-level thermodynamic fields. *Mon. Wea. Rev.,* **124,** 1767–1785.

——, and M. W. Moncrieff, 1988: The effect of large-scale convergence on the generation and maintenance of deep moist convection. *J. Atmos. Sci.,* **45,** 3606–3624.

Davies-Jones, R. D., 1979: Dual-Doppler radar coverage area as a function of measurement accuracy and spatial resolution. *J. Appl. Meteor.,* **18,** 1229–1233.

Dirks, R., 1969: A theoretical investigation of convective patterns in the lee of the Colorado Rockies. Atmos. Sci. Pap. No 145, Dept. of Atmos. Sci., Colorado State University. [Available from Dept. of Atmos. Sci., Colorado State University, Ft Collins, CO 80523.]

Dudhia, J., and M. W. Moncrieff, 1987: A numerical simulation of quasi-stationary convective bands. *Quart. J. Roy. Meteor. Soc.,* **113,** 929–967.

Fovell, R. G., and Y. Ogura, 1988: A numerical simulation of a midlatitude squall line in two dimensions. *J. Atmos. Sci.,* **45,** 3846–3879.

——, and P. S. Dailey, 1995: The temporal behavior of simulated multicell-type storms. Part I: Modes of behavior. *J. Atmos. Sci.,* **52,** 2073–2095.

Fritsch, J. M., R. J. Kane, and C. R. Chelius, 1986: The contribution of mesoscale convective weather systems to the warm-season precipitation in the United States. *J. Climate Appl. Meteor.,* **25,** 1333–1345.

Gamache, J. F., and R. A. Houze Jr., 1982: Mesoscale air motions associated with a tropical squall line. *Mon. Wea. Rev.,* **110,** 118–135.

Goff, R. C., 1974: Vertical structure of thunderstorm outflows. *Mon. Wea. Rev.,* **104,** 1429–1440.

Houze, R. A., and P. V. Hobbs, 1982: Organization and structure of precipitating cloud systems. *Advances in Geophysics,* Vol. 24, Academic Press, 225–315

——, S. A. Rutledge, M. I. Biggerstaff, and B. F. Smull, 1989: Interpretation of Doppler weather radar displays of mid-latitude mesoscale convective systems. *Bull. Amer. Meteor. Soc.,* **70,** 608–619.

——, B. F. Smull, and P. Dodge, 1990: Mesoscale organization of springtime rainstorms in Oklahoma. *Mon. Wea. Rev.,* **118,** 613–654.

Johnson, R. H., and P. J. Hamilton, 1988: The relationship of surface pressure features to the precipitation and airflow structure of an intense midlatitude squall line. *Mon. Wea. Rev.,* **116,** 1444–1472.

Klimowski, B. A., 1994: Initiation and development of rear inflow within the 28–29 June 1989 North Dakota mesoconvective system. *Mon. Wea. Rev.,* **122,** 765–779.

Leary, C. A., and R. A. Houze, 1979: The structure and evolution of convection in a tropical cloud cluster. *J. Atmos. Sci.,* **36,** 437–457.

Maddox, R. A., 1980: Mesoscale convective complexes. *Bull. Amer. Meteor. Soc.,* **61,** 1374–1387.

McAnelly, R. L., and W. R. Cotton, 1986: Meso-β-scale characteristics of an episode of meso-α-scale convective complexes. *Mon. Wea. Rev.,* **114,** 1740–1770.

Menard, R. D., and J. M. Fritsch, 1989: An MCC-generated inertially stable warm core vortex. *Mon. Wea. Rev.,* **117,** 1237–1261.

Miller, M. J., and M. W. Moncrieff, 1983: Dynamics and simulation of organized deep convection. *Proc. NATO Adv. Study Inst. Mesoscale Meteorol.—Theory Observations, Models,* Reidel, 451–496.

Moncrieff, M. W., and M. J. Miller, 1976: The dynamics and simulation of tropical cumulonimbus and squall lines. *Quart. J. Roy. Meteor. Soc.,* **102,** 373–394.

Nachamkin, J. E., R. L. McAnelly, and W. R. Cotton, 1994: An observational analysis of a developing convective complex. *Mon. Wea. Rev.,* **122,** 1168–1188.

Neiman, P. J., P. T. May, B. B. Stankov, and M. A. Shapiro, 1991: Radio acoustic sounding system observations of an arctic front. *J. Appl. Meteor.,* **30,** 881–892.

Newton, C. W., 1950: Structure and mechanism of the prefrontal squall line. *J. Meteor.,* **7,** 210–222.

Ogura, Y., and M.-T. Liou, 1980: The structure of a midlatitude squall line: A case study. *J. Atmos. Sci.,* **37,** 553–567.

Rotunno, R., J. B. Klemp, and M. L. Weisman, 1988: A theory for strong, long-lived squall lines. *J. Atmos. Sci.,* **45,** 463–485.

Schmidt, J. M., and W. R. Cotton, 1989: A high plains squall line associated with severe surface winds. *J. Atmos. Sci.,* **46,** 281–302.

——, and ——, 1990: Interactions between upper and lower tropospheric gravity waves on squall line structure and maintenance. *J. Atmos. Sci.,* **47,** 1205–1222.

Skamarock, W. C., M. L. Weisman, C. A. Davis, and J. B. Klemp, 1994: Three-dimensional evolution of simulated long-lived squall lines. *J. Atmos. Sci.,* **51,** 2563–2584.

Smull, B. F., and R. A. Houze Jr., 1985: A midlatitude squall line with a trailing region of stratiform rain: Radar and satellite observations. *Mon. Wea. Rev.,* **113,** 117–133.

——, and ——, 1987a: Dual-Doppler radar analysis of a mid-latitude squall line with a trailing region of stratiform rain. *J. Atmos. Sci.,* **44,** 2128–2148.

——, and ——, 1987b: Rear inflow in squall lines with trailing stratiform precipitation. *Mon. Wea. Rev.,* **115,** 2869–2889.

Stensrud, D. J., and J. M. Fritsch, 1994: Mesoscale convective systems in weakly forced large-scale environments. Part I: Observations. *Mon. Wea. Rev.,* **121,** 3326–3344.

——, R. A. Maddox, and C. L. Ziegler, 1991: A sublimation-initiated mesoscale downdraft and its relation to the wind field below a precipitating anvil cloud. *Mon. Wea. Rev.,* **119,** 2124–2139.

Strauch, R. G., D. A. Merrit, K. P. Moran, K. B. Earnshaw, and D. van de Kamp, 1984: The Colorado wind profiling network. *J. Atmos. Oceanic Technol.,* **1,** 37–49.

Sun, J., S. Braun, M. I. Biggerstaff, R. G. Fovell, and R. A. Houze Jr., 1993: Warm upper-level downdrafts associated with a squall line. *Mon. Wea. Rev.,* **121,** 2919–2927.

Szoke, E. J., M. L. Weisman, J. M. Brown, F. Caracena, and T. W. Schlatter, 1984: A subsynoptic analysis of the Denver tornadoes of 3 June 1981. *Mon. Wea. Rev.,* **112,** 790–808.

Thorpe, A. J., M. J. Miller, and M. W. Moncrieff, 1982: Two-dimensional convection in nonconstant shear: A model of midlatitude squall lines. *Quart. J. Roy. Meteor. Soc.,* **108,** 739–762.

Tripoli, G. J., and W. R. Cotton, 1989: Numerical study of an observed orogenic mesoscale convective system. Part I: Simulated genesis and comparison with observations. *Mon. Wea. Rev.,* **117,** 273–304.

Wallace, J. M., 1975: Diurnal variations in precipitation and thunderstorm frequency over the conterminous United States. *Mon. Wea. Rev.,* **103,** 406–419.

Weisman, M. L., 1992: The role of convectively generated rear-inflow jets in the evolution of long-lived mesoconvective systems. *J. Atmos. Sci.,* **49,** 1826–1847.

——, and J. B. Klemp, 1982: The dependence of numerically simulated convective storms on vertical wind shear and buoyancy. *Mon. Wea. Rev.,* **110,** 504–520.

——, J. B. Klemp, and R. Rotunno, 1988: Structure and evolution of numerically simulated squall lines. *J. Atmos. Sci.,* **45,** 1990–2013.

Zipser, E. J., 1977: Mesoscale and convective-scale downdrafts as distinct components of squall line structure. *Mon. Wea. Rev.,* **105,** 799–814.